Detection of weak lensing by a cluster of galaxies at $z = 0.83$

G. A. Luppino

Institute for Astronomy, University of Hawaii

2680 Woodlawn Drive, Honolulu, Hawaii 96822, email: ger@hokupa.ifa.hawaii.edu

AND

Nick Kaiser[1]

Canadian Institute for Advanced Research and Canadian Institute for Theoretical Astrophysics

University of Toronto, 60 St. George St., Toronto, Canada M5S 1A7, email: kaiser@cita.utoronto.ca

Abstract

We report the detection of weak gravitational lensing of faint, distant background galaxies by the rich, X-ray luminous cluster of galaxies MS 1054−03 at $z = 0.83$. This is the first measurement of weak lensing by a bona fide cluster at such a high redshift. We detect tangential shear at the 5% - 10% level over a range of radii $50'' \lesssim r \lesssim 250''$ centered on the optical position of the cluster. Two-dimensional mass reconstruction using galaxies with $21.5 < I < 25.5$ shows a strong peak which coincides with the peak of the smoothed cluster light distribution. Splitting this sample by magnitude (at $I = 23.5$) and color (at $R - I = 0.7$), we find that the brighter and redder subsamples are only very weakly distorted, indicating that the faint blue galaxies (FBG's), which dominate the shear signal, are relatively more distant. The derived cluster mass is quite sensitive to the $N(z)$ for the FBG's. At one extreme, if all the FBG's are at $z_s = 3$, then the mass within a $0.5h^{-1}$Mpc aperture is $(5.9 \pm 1.24) \times 10^{14}h^{-1} \ M_\odot$, and the mass-to-light ratio is $M/L_V = 350 \pm 70h$ in solar units. For $z_s = 1.5$ the derived mass is $\sim 70\%$ higher and $M/L \simeq 580h$. If $N(z)$ follows the no evolution model (in shape) then $M/L \simeq 800h$, and if all the FBG's lie at $z_s \lesssim 1$ the required M/L exceeds $1600h$. These data provide clear evidence that large, dense mass concentrations existed at early epochs; that they can be weighed efficiently by weak lensing observations; and that most of the FBG's are at high redshift.

Subject headings: cosmology: observations — gravitational lensing — dark matter — galaxies: photometry — galaxies: distances and redshifts — galaxies: clusters: individual (MS 1054−03).

1. Introduction

The technique of weak gravitational lensing has emerged as a powerful probe both of clusters of galaxies and of the faint blue galaxy [FBG] population. Most weak lensing observations to date have concentrated on low and intermediate redshift clusters ($z \sim 0.2$–0.4); for example A1689 at $z = 0.18$ (Tyson, Valdes & Wenk 1990; Tyson & Fischer 1995; Kaiser, Broadhurst, Szalay and Moller, 1996), A2218 at $z = 0.18$ (Squires et al. 1995), MS1224+24 at $z = 0.33$ (Fahlman et al. 1994), A370 at $z = 0.375$ (Kneib et al. 1994), and Cl 0024+17 at $z = 0.39$ (Bonnet et al. 1994). Clusters in this redshift range are sufficiently far away that they can be imaged efficiently with existing 2048^2 pixel CCD detectors, and yet are close enough that the derived mass is little affected by uncertainty in the redshifts of the faint lensed galaxies.

---

[1]Temporarily on leave at Anglo-Australian Observatory, Epping Laboratory, NSW 2121, Australia

Observing lensing by high-redshift ($z > 0.7$) clusters is more difficult, since for a lens of a given mass the distortion tends to weaken with increasing lens redshift, especially as the lens redshift approaches that of the sources. However, this dependence of the distortion strength on the observer-lens-source geometry potentially provides a powerful constraint on the redshift distribution $N(z)$ of faint galaxies. If the majority of these lie at high redshift ($z > 2$, say), then we should see strong distortion for even the most distant ($z \sim 1$) clusters, but if the majority of faint galaxies lie at or below $z \sim 1$, then the distortion should fall rapidly as the cluster redshift approaches unity. In this way, one can constrain $N(z)$ at much fainter magnitudes ($I > 24$) than are accessible by spectroscopic surveys, even with the new generation of 8–10 m telescopes.

Smail et al. (1994) tried this experiment by looking for weak lensing in three clusters covering a wide range of redshifts ($z = 0.26$, $z = 0.55$ and $z = 0.89$). A clear lensing signature was seen in the $z = 0.26$ cluster, and a somewhat weaker signal in the $z = 0.55$ cluster, but none was seen in the highest redshift cluster, Cl 1603+43 at $z = 0.89$, suggesting that the majority of FBGs with $I < 25$ were at $z \lesssim 1$. However, an alternative interpretation is that Cl 1603+43 is simply not massive enough to produce a measurable shear signal. This is not implausible since this cluster was optically selected (Gunn et al. 1986), and has an X-ray luminosity of only $L_x \sim 1 \times 10^{44}$ erg s^{-1}; (Castander et al. 1994), as compared to the two lower-redshift clusters which both have $L_x > 10^{45}$ erg s^{-1}. Of course, Smail et al. had little to choose from. When they performed their observations, there were no known clusters at $z > 0.7$ with X-ray luminosities comparable to the richest and brightest low-redshift clusters, and the small number of high-z clusters then known were mainly optically detected (e.g. Gunn et al. 1986; Couch et al. 1991). Recently, however, several new, high-redshift clusters have been discovered as the optical counterparts to previously-unidentified *Einstein* Extended Medium Sensitivity Survey (EMSS) X-ray sources (Gioia et al. 1990; Gioia & Luppino 1994). The most distant of these, MS 1054−03 at $z = 0.83$, is extremely rich and has an X-ray luminosity an order of magnitude higher than Cl 1603+43 (Luppino & Gioia 1995), suggesting it may be a potent gravitational lens.

In this paper, we report the detection of weak gravitational lensing by MS 1054−03. Our observations and data reduction are outlined in §2, the cluster properties are described in §3. In §4, we apply weak lensing analysis, and in §5, we discuss the implications of our observations for cosmological structure formation models, and for the constraining the redshift distribution of the faint background galaxies.

2. Observations and data reduction

Optical R and I-band images of MS 1054−03 were obtained with the UH 2.2m telescope on the nights of 19 Feb 1993 and 11-13 Jan 1994. A thinned Tek 2048^2 CCD was mounted at the f/10 RC focus resulting in a scale of 0″.22/pixel and a field of view of 7′.5×7′.5 (physical scale 1.86h^{-1}Mpc at $z = 0.83$). The total exposure times were 7200 s and 21600 s in R and I respectively. The individual images in each filter were first de-biased and then flattened using a median of all the CCD frames taken in that filter (including the cluster images which made up $\sim {}^1/_3$ of the total number of frames). Low spatial frequency residual sky fluctuations were then removed by subtracting a highly smoothed image determined from the troughs of the minima in the images. Registration was performed using ~ 50 moderately bright stars, and the images were then transformed to a common coordinate system (with bi-linear interpolation). The stack of transformed images was then summed with cosmic-ray rejection and using appropriate weights (the cosmic-ray rejection being done in such a way as to ensure that the effective psf for the stars was the same as for the faint objects). The seeing in the resulting R and I images was 1″.14 and 0″.97 FWHM respectively. Photometric calibration was performed using the standard stars of Landolt (1993). The variation in extinction between the I-band images was very small, as was also the case for all but three of the R-band images. The 1σ surface brightness limits of the summed R and I images are 27.9 mag arcsec^{-2} and 27.8 mag arcsec^{-2} respectively.

In order to detect the faint objects we used the algorithm of Kaiser, Squires & Broadhurst (1995 [KSB]). This provides a catalog with accurate positions but crude size and magnitude information. We then used

this catalog to mask the summed images and thus determine and subtract the small residual positive bias in the images left by the local sky subtraction, and we then applied photometric analysis to obtain refined sizes, magnitudes etc. The resulting catalog contained some noise peaks as well as detections of groups of objects. These were removed by limiting the catalog at 5-sigma detections and removing abnormally small and large objects. We also rejected a small number of objects with high eccentricity to obtain final catalogs containing $N_I = 2718$ and $N_R = 1822$ objects, corresponding to about 1.7×10^5 and 1.2×10^5 objects per square degree. Nearly all the objects detected in the R-band were also detected in I. The I-magnitudes were determined using a large aperture $r_{\rm ap} = 3r_g$, where r_g is the smoothing scale at which the object was detected, and typically overestimate total magnitudes by $\lesssim 0.1$ mag.

3. Cluster properties

MS 1054−03 is an extraordinary object. It is by far the richest and most X-ray luminous high-redshift ($z > 0.7$) cluster known, and is among the richest clusters known at any redshift. A true color image centered on the $I = 19.3$ brightest cluster galaxy (BCG) is shown in figure 1 [Plate 1]; the cluster is easily identified as the horizontal swath of red galaxies in the center of the frame. Figure 2 shows the location, I-magnitude and color of all the non-stellar objects with $I < 24.5$ and with colors in the range $1.93 > R - I > 1.1$ which brackets the color of the cluster galaxies. The total magnitude for all of the galaxies contained within a $1'$ aperture (physical scale of $\simeq 0.25h^{-1}$Mpc for $q_0 = 0.5$) centered on the brightest cluster galaxy is $I = 16.5$. Converting the observed I-band magnitude to a rest-frame solar luminosity $L_{V\odot}$ using the relation $M_V = I - 5 \log [(1 + z_l)^2 D_l] - 25 + (V - I)_{\rm o} - K(z)$ with the K-correction $K(z){=}0.85$, $(V - I)_{\rm o} = 1.3$, and $M_{V\odot} = +4.83$ we obtain $L(< 0.25h^{-1}\,{\rm Mpc}) = 1.19 \times 10^{12} L_{V\odot}$, which includes a $\sim 15\%$ contribution from the bright foreground galaxy lying $\sim 1'$ to the north of the cluster center. For a $0.5h^{-1}$Mpc aperture we find $L(< 0.5) = 2.0 \times 10^{12} L_{V\odot}$. The number of galaxies with $I < 22$ counted within the same apertures
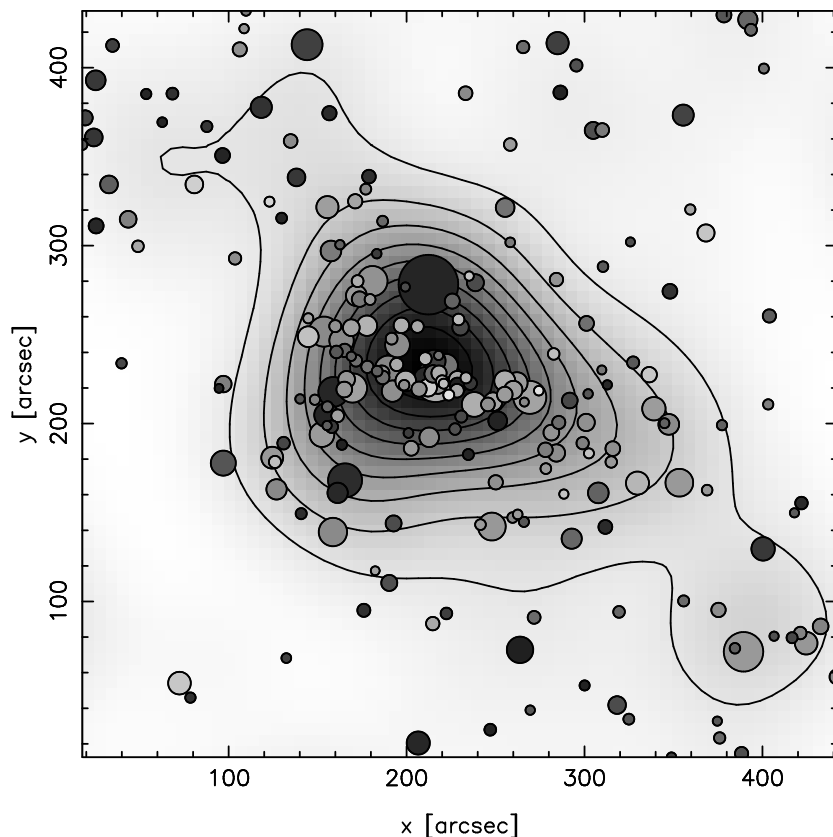

FIGURE 2. Spatial distribution of red galaxies (including the sequence of cluster galaxies with $R - I \simeq 1.5$). The size of each circle is proportional to the brightness of the galaxy (in I), and the shading indicates the color on a scale of $R - I = 1.9$ (white) to $R - I = 1.1$ (black). The underlying gray-scale is the I-band surface brightness smoothed with a $35''$ gaussian filter.

are $N(<0.25) = 49$ and $N(<0.5) = 82$, which represent an excess over the background of about 44 and 67 galaxies respectively, making this at least a richness class 4 cluster (Bahcall 1981).

Although MS 1054−03 is clearly very X-ray luminous ($L_{0.3-3.5\,\mathrm{keV}} = 9.3 \times 10^{44}\ h_{50}^{-2}$ erg s^{-1}), the actual X-ray flux is quite low because the cluster is so distant, and consequently little can be said about its X-ray properties at the present time. MS 1054−03 was unresolved in the *Einstein* IPC with only 107.9±12.8 counts in an 18 ksec exposure, corresponding to a flux of $f_x = 2.11 \times 10^{-13}$ erg cm^{-2} s^{-1} (Henry et al. 1992). The flux was converted to a luminosity assuming a 6 keV thermal spectrum and correcting for extended emission as outlined in Gioia & Luppino (1994). An *ASCA* spectrum has recently been obtained, and a preliminary analysis indicates the cluster has a high X-ray temperature (Donahue, private communication). ROSAT HRI observations are scheduled.

4. Weak lensing analysis

The weak lensing analysis involves several steps. Object polarizations $e_\alpha = \{I_{11} - I_{22}, 2\, I_{12}\}/(I_{11} + I_{22})$ were formed from the the quadrupole moments $I_{ij} = \int d^2\theta\, W(\theta)\theta_i\theta_j f(\theta)$ where f is the flux density and $W(\theta)$ is a gaussian weighting function matched to the size of the galaxy. We then extract a sample of moderately bright stars which have non-zero polarization due to anisotropy of the point spread function, fit a low order polynomial model for the psf variation across the field, and then correct the galaxy polarizations for all the objects to what they would have been for perfectly circular seeing as described in KSB. These e_α values should now be equal to the random intrinsic values plus a small coherent shift which is proportional to the gravitational shear $\gamma_\alpha = \frac{1}{2}\{\phi_{,11} - \phi_{,22}, 2\phi_{,12}\}$ where ϕ is related to the dimensionless surface mass density by $\kappa = \Sigma/\Sigma_{crit} = \frac{1}{2}\nabla^2\phi$ and where the critical density $\Sigma_{crit}^{-1} = 4\pi G c^{-2} D_l D_{ls} D_s^{-1} = 4\pi G c^{-2} D_l \beta$, with $\beta \equiv D_{ls}/D_s \ (= [1 - D_l(1+z_l)/D_s(1+z_s)])$ for $\Omega = 1$).

The next step is to calibrate the relation between the polarization and the shear. Previously, this has been done by artificially shearing deep HST images to simulate lensing and convolving with a gaussian seeing disk (KSB). Here we have used a slightly different approach. We artificially shear the actual I-band image (which is equivalent to shearing the image as it would appear from space, but then convolving with a slightly anisotropic psf), and then correct the galaxy polarizations using the sheared stars. This is equivalent (for small shear at least) to shearing the image before seeing and then smoothing with a circular psf, and the shear polarisability is then just equal to the change in the polarization divided by the applied shear, $P_\gamma = de/d\gamma$. The individual P_γ values are rather noisy for the faintest objects, but the mean polarisability varies smoothly in the way expected with radius, and should be adequate to determine the appropriate calibration factor $\langle P_\gamma \rangle$ for each of the subsamples we will construct. This new approach gives results which agree very well with those from the previous method using HST images (KSB), but is more convenient here. We now have a fair estimate of the shear $\hat{\gamma}_\alpha = e_\alpha/\langle P_\gamma \rangle$ for each galaxy — albeit a rather noisy one — which we now analyze in a number of different ways, and also using various subsamples.

First we define a sample of all faint objects in the I catalog having $I > 21.5$ (2395 objects). No attempt was made to remove stars or cluster galaxies. This faint galaxy sample can be seen in figure 3 [Plate 2] as ellipses overlaid on the I-band CCD image of the cluster. Figure 4 shows the result of applying two different inversion algorithms to recover the dimensionless surface density $\kappa(\vec{r})$: the original Kaiser & Squires (1993) algorithm [KS93] and the new, unbiased Squires & Kaiser (1996) algorithm [SK96]. Massmaps generated by either algorithm (see figs 4a and 4c) show strong mass concentrations very close to the peak of the smoothed lightmap. Also shown are reconstructions using the same spatial distribution, but with random gaussian shear values with $\langle \gamma_\alpha^2 \rangle^{1/2} = 0.6$ (a value determined from the data as described below). These mass reconstructions have been smoothed to the same $35''$ gaussian filter scale as the light. Figure 5 [Plate 3] shows a contour plot (white contours) of the cluster light superimposed on the mass contours (black contour lines) overlaid on the I-band CCD image of the cluster field.

While the relation between the shear (essentially the tidal field) and κ is a non-local one, there is an
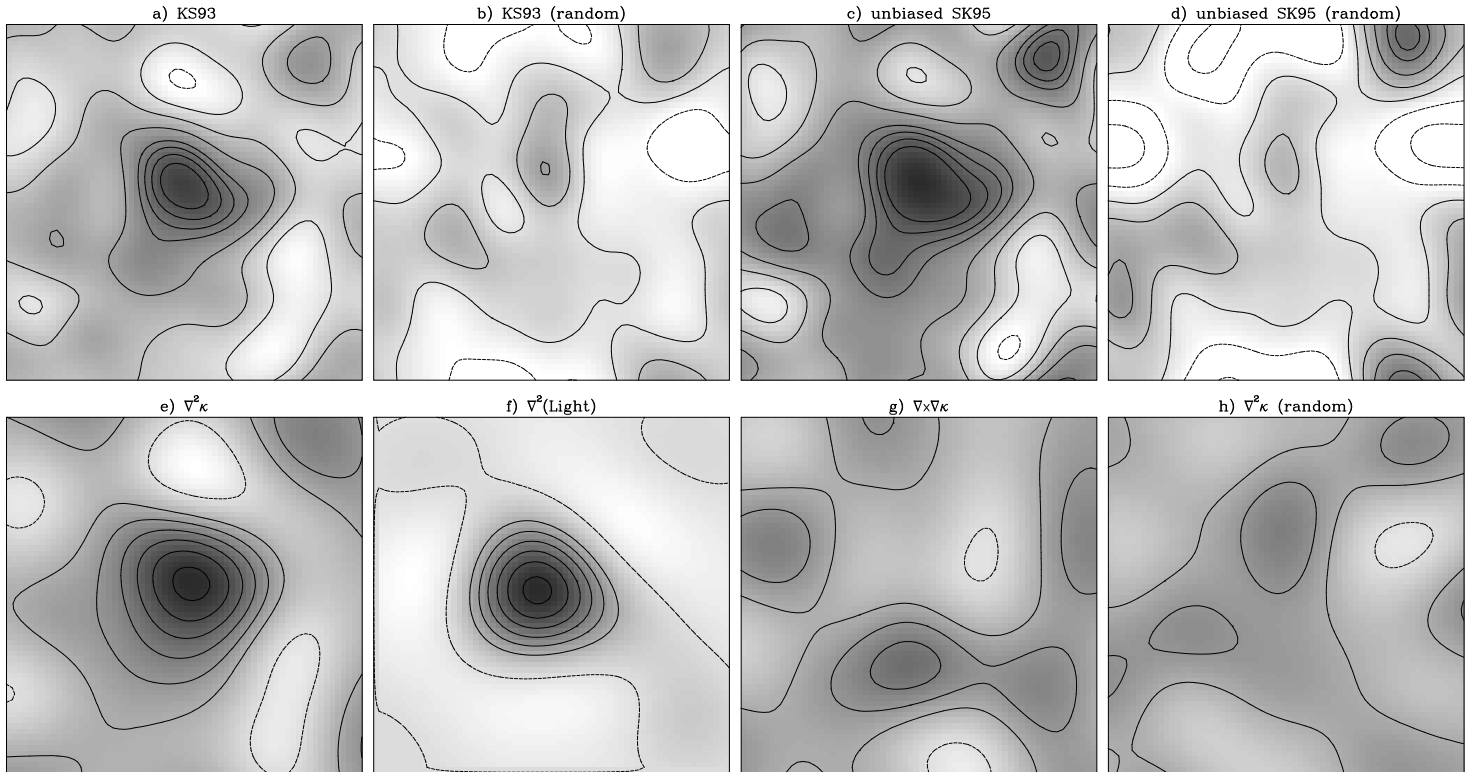
FIGURE 4. The top four panels show the result of two different mass reconstruction algorithms: a) the original KS93 method and c) the new, unbiased 'regularized maximum likelihood' technique of Squires & Kaiser (1996). While the KS93 method is susceptible to a slight negative bias at the edge of the field (Schneider 1995), it appears that in this case any bias that might be present is small. Panels b) and d) are reconstructions using a catalog in which the galaxies were assigned normally distributed random shear values with rms (per component) $\gamma_\alpha = 0.6$, and which indicate the expected level of noise in these reconstructions. The lower four panels contain e) a smoothed image of $\nabla^2\kappa$ (or equivalently κ smoothed with a compensated 'mexican-hat' filter), f) the Laplacian of the surface brightness (scaled to have the same peak value), g) an estimate of $\nabla \times \nabla\kappa$ which should be zero if the shear field is really due to gravity, and h) a realization of the noise produced by our random catalog.

explicit local expression for the gradient of the surface density in terms of the gradients of the shear (Kaiser 1995), and one can therefore determine $\nabla^2\kappa$, the Laplacian of the surface density, from local shear estimates. A smoothed image (filter scale = $70''$) of $\nabla^2\kappa$ is shown in figure 4e. The smoothed Laplacian is just the surface density convolved with a particular form of 'mexican-hat' smoothing filter — it is because this filter is 'compensated' that the resulting field does not suffer from the slight bias (Schneider 1995) inherent in the KS93 method, and so can be compared directly with the Laplacian of the surface brightness (figure 4f); clearly these agree in shape and location very well indeed.

An interesting feature of this kind of analysis is that it provides a powerful check on whether the distortion we are detecting is really due to gravitational lensing. If instead of the Laplacian $\nabla \cdot \nabla\kappa$ we calculate the curl of the gradient $\nabla \times \nabla\kappa$, we should then get zero plus fluctuations due to the random noise in the shear estimates. What we are doing here is exploiting the fact that while a general distortion field has two real degrees of freedom, one generated by gravity has only one, and we are projecting out two components of the shear field: one which is excited by gravitational lensing and another which is not. To generate $\nabla \times \nabla\kappa$
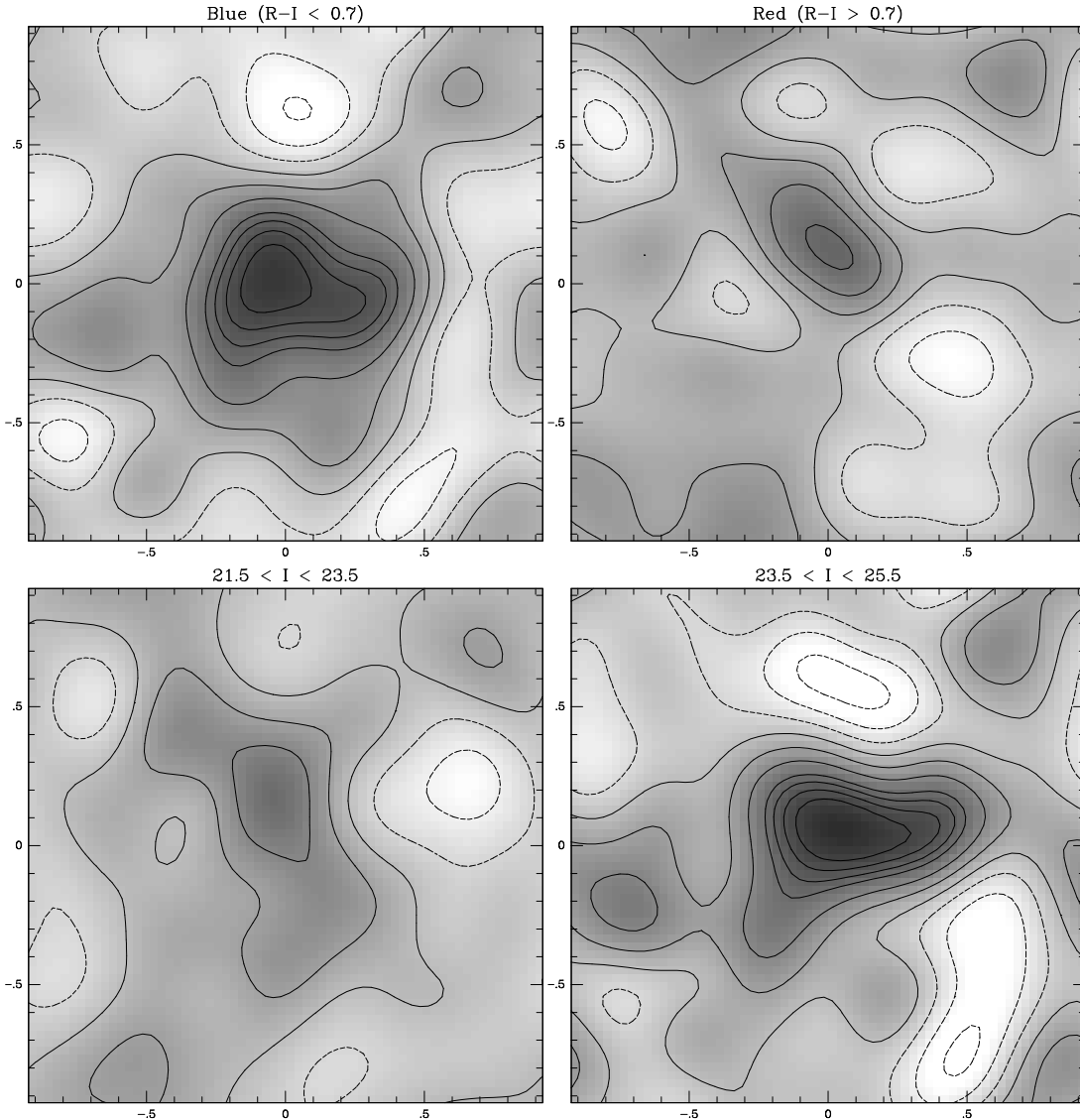
FIGURE 6. Mass reconstruction from the various galaxy subsamples: upper left, blue; upper right, red; lower left, faint-bright galaxies ($21.5 < I < 23.5$); lower right, faint-faint galaxies ($23.5 < I < 25.5$). The axes are labeled in units of h^{-1} Mpc. All four massmaps are displayed with the same intensity stretch and contour levels.

rather than $\nabla \cdot \nabla \kappa$ we simply swap the two components of the shear and change the sign of one of them (this is equivalent to rotating each object by 45 degrees). Due to the high symmetry of these operations, one would expect most (but not necessarily all) artificial sources of distortion to excite both modes, and so the smallness of the estimate of $\nabla \times \nabla \kappa$ (visible in figure 4g) provides a non-trivial check of the reality of the shear field we detect. Finally, the amplitude of the noise fluctuations expected are indicated in the lower right panel of figure 4, and we see no excess of noise due to artificial sources of image polarization (such as errors in the registration).

To search for variation in the distance to the background galaxies we have split the full $I > 21.5$ sample into subsamples by magnitude (at $I = 23.5$) and color (at $R - I = 0.7$). The mass reconstructions for these four (bright, faint, red, blue) subsamples are shown in figure 6. The faint and blue reconstructions are very similar. They clearly show the cluster, which now appears elongated in the same sense as the cluster

galaxies, and give a somewhat higher peak than for the full sample (though at a similar 5-sigma level of significance). The red and bright subsamples, however, show very little sign of the cluster at all — as would be expected if the typical redshift of these objects is less than or of order unity. Note that the difference in amplitude is not a result of different sizes for the background galaxies, as this is corrected for when we calculate P_γ; the difference must reflect a greater distance to the faint and blue objects.

In addition to the 2D mass reconstruction we have performed "aperture mass densitometry". The statistic

$$\zeta(r) = (1 - r^2/r_{\max}^2)^{-1} \int_r^{r_{\max}} <\gamma_T> d\ln r \qquad (1)$$

(Kaiser et al. 1995; Fahlman et al. 1994) measures $\overline{\kappa}(r)$, the mean surface mass density interior to r, minus the mean surface density in the annulus from r to $r_{\max}$, and therefore provides a lower bound on $\overline{\kappa}$ and hence on the mass within an aperture of radius r. Here, the tangential shear is $<\gamma_T> = \frac{1}{2\pi} \int \gamma_T \, d\varphi$, where $\gamma_T = \gamma_1 \cos 2\varphi + \gamma_2 \sin 2\varphi$, and φ is the azimuthal angle with respect to some chosen center (which we have taken to be the peak of the smoothed light image in figure 2).

The tangential shear and $\zeta(r)$ are shown for the various subsamples in figure 7. A coherent tangential shear pattern is clearly seen in the $I > 21.5$ sample over a range of radii from $\sim 50''$ to $\sim 300''$ (though we do not have full azimuthal coverage for $r > 220''$), and the ζ-statistic shows that the mean dimensionless surface density rises to $\overline{\kappa} \simeq 0.25$ at $r \simeq 60''$ with a fractional statistical error of about 20%. We calculate the variance in $\gamma_\times \equiv -\gamma_1 \sin 2\varphi + \gamma_2 \cos 2\varphi$. If the shear pattern is circularly symmetric then this should give a fair estimate of the statistical uncertainty in the shear estimates, and the error bars in figure 7 are based on this estimate. For the $I > 21.5$ sample for instance, we obtain $\langle \gamma_\times^2 \rangle^{1/2} \simeq 0.6$ which is the value used in the 'noise reconstructions' of figure 4. The γ estimates have uncorrelated statistical uncertainty, whereas the ζ estimates are somewhat correlated (as we have used logarithmically spaced bins in r, each ζ-estimate is just a sum of the γ estimates which lie at larger radii, thus ζ estimates at small r tend to have errors which are quite strongly correlated). We should emphasize that because we have taken the spatial origin to be the brightest cluster galaxy, the errors in both γ and ζ are unbiased, and it is equally likely that we have over- or under-estimated the mass.

The lower panels in figure 7 show graphically how the distortion strength varies with color and magnitude of the background objects. The tangential shear is barely seen in the bright and red subsamples, while for the faint and blue samples, γ_T lie roughly 30% higher than the full $I > 21.5$ sample and gives $\overline{\kappa}(< 0.25) \simeq 0.35 \pm 0.07$ and $\overline{\kappa}(< 0.5) \simeq 0.20 \pm 0.06$. For the bright and red subsamples the values are 0.13 ± 0.07 and 0.07 ± 0.05, and this *difference* (in shear values between red and blue or bright and faint subsamples) is significant at the $\simeq 2.2$-sigma level. These values are unlikely to have been significantly affected by cluster contamination, since they only make use of data outside the aperture.

The average physical surface mass density is obtained by multiplying $\overline{\kappa}$ (or ζ) by the critical density, Σ_{crit}, and a lower limit to the total projected mass within r is then $M(< r) > \pi r^2 \zeta(r) \Sigma_{crit} = c^2 r^2 \zeta/(4GD_l\beta)$. The big uncertainty here is the value for β, which varies by a factor of ~ 5 from $\beta \sim 0.1$ if all the FBGs are at $z_s \sim 1$ to $\beta \sim 0.5$ if the FBGs are at the maximum plausible redshift of $z_s \sim 3$ (Guhathakurta et al. 1990). The critical surface density is $\Sigma_{\rm crit} = 1.95 \times 10^{15} \beta^{-1} M_\odot h \text{Mpc}^{-2}$ and ranges from $1.7 \times 10^{16} \, h \, M_\odot \, \text{Mpc}^{-2}$ to $3.9 \times 10^{15} \, h \, M_\odot \, \text{Mpc}^{-2}$ over this range of source redshifts. If the FBG $N(z)$ shape follows the no evolution model (as used in Glazebroook et al., 1995) then $\beta \simeq 0.22$ and $\Sigma_{\rm crit} = 8.8 \times 10^{14} M_\odot h \text{Mpc}^{-2}$.

In figure 8 we plot the cluster radial mass profile for three different values of β corresponding to the faint lensed galaxies lying on sheets at $z_s = 1$, 1.5, and 3. Also shown for comparison are isothermal sphere mass profiles with velocity dispersions 2200, 1450, and 1100 km/s. A conservative lower bound on the cluster mass is obtained if we assume that the faint/blue galaxies lie at $z_s = 3$, and we then find $M(< 0.25) = (2.7 \pm 0.6) \times 10^{14} h^{-1} M_\odot$ and $M(< 0.5) = (5.9 \pm 1.3) \times 10^{14} h^{-1} M_\odot$. For the no-evolution $N(z)$, $M(< 0.5) = (1.39 \pm 0.29) \times 10^{15} h^{-1} M_\odot$.
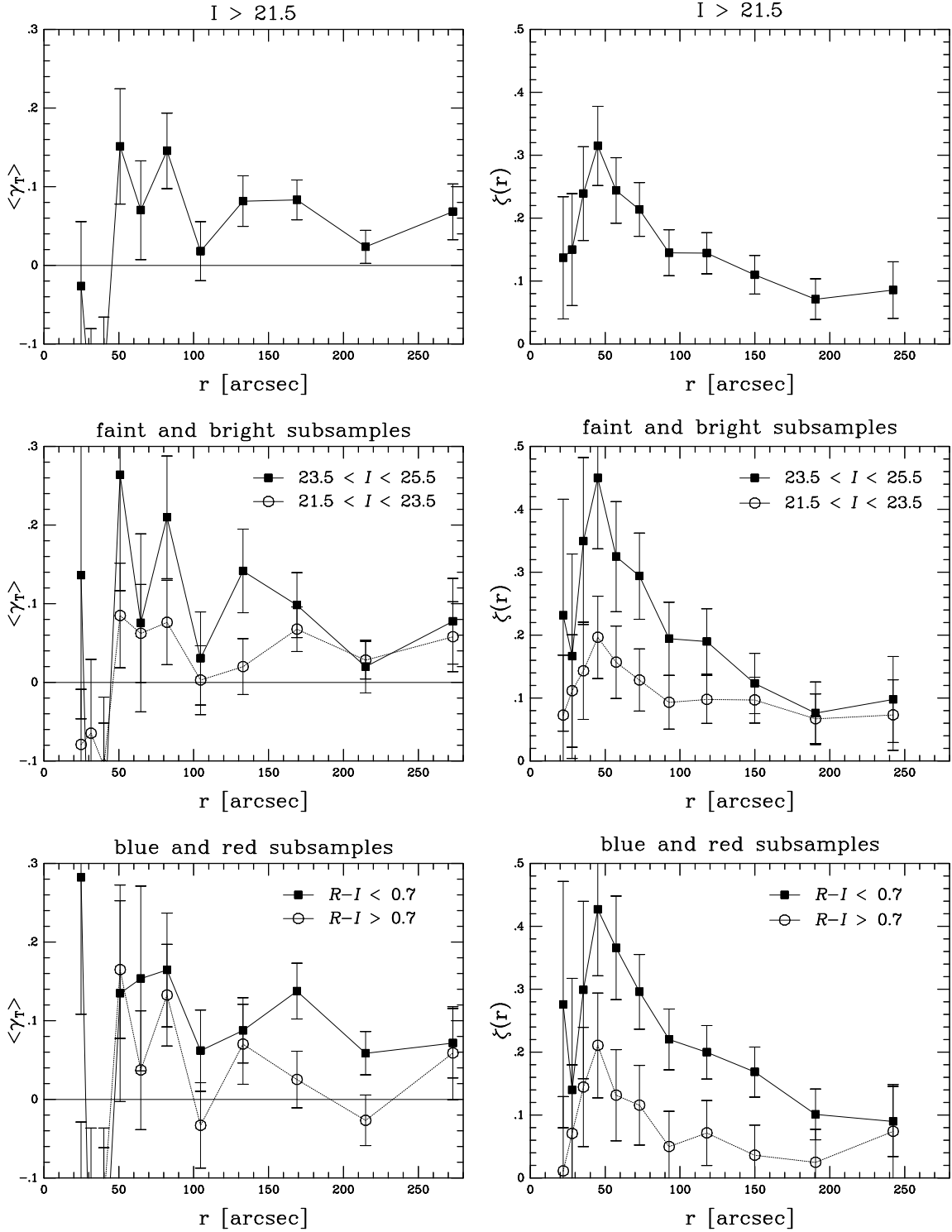
FIGURE 7. Panels on the left show the tangential shear γ_T for the $I > 21.5$ sample (top); the faint and bright subsamples are shown as square and circular symbols in the middle panel and the blue (square) and red (circle) samples are shown in the bottom panel. The righthand panels show $\zeta(r)$ which provides a lower bound on $\overline{\kappa}(r)$.
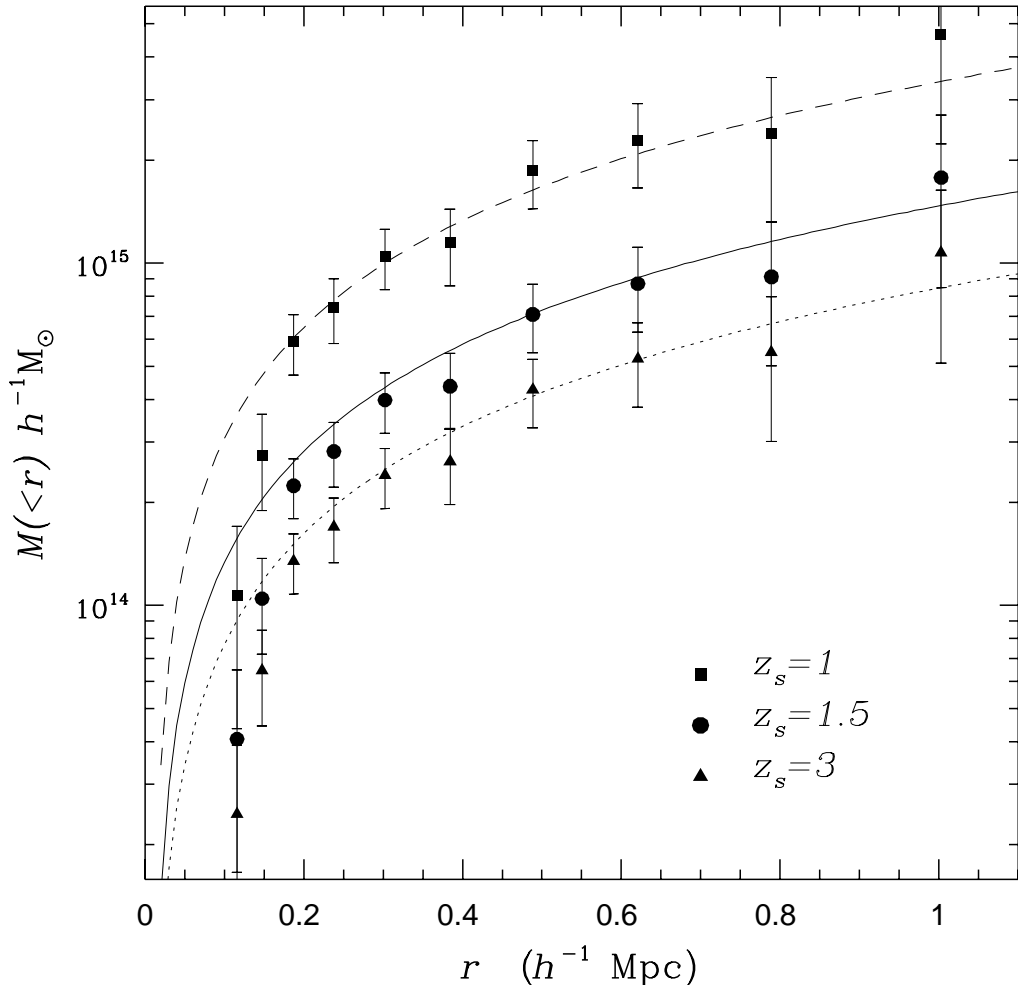
FIGURE 8. Plot of the radial mass profile $[M(< r) > \pi r^2 \kappa(r) \Sigma_{crit} = c^2 r^2 \overline{\kappa}/(4GD_l\beta)]$ of MS 1054−03 using the κ (or ζ) values from the $I > 21.5$ sample for three different values of β assuming the faint lensed galaxies lie on sheets at $z_s = 1$, $z_s = 1.5$, and $z_s = 3$. The errorbars only reflect the errors in $\overline{\kappa}$, and not the uncertainty in Σ_{crit}. The dashed, solid and dotted lines are mass profiles for isothermal spheres with $\sigma = 2200$, 1450, and 1100 km/s respectively.

We can combine these projected mass estimates with the projected light estimates of §3 to obtain the cluster mass-to-light ratio. Since the mass estimates really measure the mean surface density in the aperture relative to that in the surrounding annulus we reduce the luminosity estimates by the expected mean surface brightness (this is a small correction; roughly 5% and 15% for the smaller and larger apertures respectively). If we place the faint/blue galaxies at $z_s = 3$ then we obtain $M/L_V \simeq 250h$ for the small aperture and $M/L_V \simeq 350h$ for the larger (with $\simeq 21\%$ statistical uncertainty). If instead they lie at $z_s = 1.5$, then the mass increases by roughly 70% and the mass-to-light ratio (for the $0.5h^{-1}$Mpc aperture) rises to $M/L_V \simeq 580$. For the no evolution $N(z)$ we find $M/L_V = (790 \pm 170)h$ and for $z_s < 1$ we would require $M/L_V > 1600h$.

Finally, the net shear (which is sensitive to structures outside the beam) is $\gamma = \{0.019, -0.016\} \pm 0.012$, which is essentially a null detection, but at a precision level which is already at about the level of the expected signal from large-scale structure, so the prospects for constraining the large-scale mass power spectrum $P(k)$ with large angle surveys is excellent.

9

5. Discussion

These results have implications for both the properties of high-z clusters (and therefore for cosmogonical theory), and for the $N(z)$ of the FBG's.

Regarding the cluster properties, we have found that the mass-to-light ratio is $> 350h$, with the lower limit corresponding to having all the faint lensed galaxies at $z = 3$. This must be an underestimate as some of the galaxies surely lie at lower redshifts. For a more plausible mean redshift of, say $z_s = 1.5$, we obtain $M/L \simeq 580h$ (though a somewhat lower value for the central mass-to-light ratio), and for the no-evolution model $M/L \simeq 800h$. This is quite large compared to values normally obtained from the X-ray or virial analysis, but is quite consistent with values measured by weak lensing for other lower-redshift clusters (Fahlman et al. 1994; Smail et al. 1995; Tyson & Fischer 1995; Squires et al. 1995).

The high M/L coupled with the high luminosity of the cluster makes it very massive indeed — it has the same projected surface mass density as a Navarro model (Navarro, Frenk & White 1995) with rotation velocity v_{200} in the range 2400–2800 km/s, or as an isothermal sphere with line of sight velocity dispersion of 1100–2200 km/s (see figure 8). The existence of large clusters like this at high redshift is problematic for hierarchical cosmological models like CDM with $\Omega = 1$. While this problem has been recognized for some time (Evrard 1989; Peebles et al. 1989; Gunn 1990), it has not been taken too seriously because of the lack of conclusive evidence that any of the few known high-z clusters were truly massive. We now have firm evidence for at least one such system. Using the Press-Schechter approximation, the predicted comoving number density of $10^{15}h^{-1}\mathrm{M}_\odot$ clusters at $z \sim 0.8$ in a standard CDM model ($\sigma_8 = 1.1$) is at least an order of magnitude lower than the number density at $z = 0$ (Vianna & Liddle 1995). But the existence of only one $10^{15}h^{-1}\mathrm{M}_\odot$ cluster at $z \sim 0.8$ in the EMSS survey volume corresponds to a comoving number density of order $n \sim 5 \times 10^{-8}\, h^3\ \mathrm{Mpc}^{-3}$ (Luppino & Gioia 1995), comparable to the "local" density $n\,(M > 10^{15}h^{-1}\mathrm{M}_\odot\,)$ $\sim 10^{-7}\, h^3\ \mathrm{Mpc}^{-3}$ (White et al. 1993). In mixed dark matter models, the predicted abundance of massive clusters drops even more rapidly with redshift than in standard CDM.

The question of the $N(z)$ for the FBG population has been a matter of debate for some time. While some of the faint field galaxy population consists of low-redshift ($z < 0.5$) dwarfs, there remains the possibility that large, star forming galaxies at $z > 1$ make up a significant fraction of the FBG excess counts, especially at faint magnitudes (Cowie et al. 1995). There have been hints of this high redshift component to the FBGs from lensing observations of lower redshift ($z < 0.5$) clusters (Fort et al. 1992; Kneib et al. 1994), and Smail & Dickinson (1995) have reported the detection of weak shear by a putative cluster surrounding the radio galaxy 3C324 at $z = 1.2$. Furthermore, there is some weak lensing evidence for a $z \sim 1.5$ mass concentration coincident with a group of very faint galaxies that may be partly responsible for the lensing of Q2345+007 (Mellier et al. 1994; Fischer et al. 1994). On the other hand, as mentioned earlier, the failure of Smail et al. to detect lensing in Cl1603+43 might lead one to the opposite conclusion. Our observation shows unequivocally that the lensed, faint background galaxies are predominantly blue, and that the majority of these in the range $23.5 < I < 25.5$ lie at redshifts of order unity or greater. Unfortunately we cannot be more precise without some independent estimate of the mass of the cluster. What we *can* say, however, is that either extreme case is very interesting. On one hand, if the cluster has a mass-to-light ratio at the lower limit of $\sim 350h$, then nearly all of the FBG's must lie at very high redshift. On the other hand, to accomodate a more reasonable $N(z)$, such as a 'no-evolution' model, requires a mass-to-light ratio of $\sim 800h$ and the cluster would then be exceptionally massive and should have an enormous velocity dispersion and X-ray temperature (at least in so far as the cluster is approximately spherical and relaxed).

It is clear, however, that detailed information on the FBG $N(z)$ is quite within reach. What is needed is a sample of five or ten massive clusters at similar redshift to MS1054−03, along with a reasonably complete spectroscopic sample to say $I = 23$. Although, as we have seen, it is difficult to detect the lensing in the brighter galaxies, with a number of lenses the statistics will improve and we should be able to determine the relative distances for the faint galaxies relative to the brighter ones, and then use the spectroscopic redshifts

to tie down the overall scale. Ongoing spectroscopic surveys with the largest telescopes are now beginning to obtain spectra at the magnitude limits required here. Using the Keck Telescope, Cowie et al. (1996) have taken spectra of a sample of several hundred galaxies nearly complete to $I = 23$ ($K = 20$, $B = 24.5$). Interestingly, when they split their sample by color (at $B - I = 1.6$), they find that the blue galaxies divide into distinctly separate low redshift ($z \sim 0.25$) and high redshift ($z > 0.8$) populations, with the bulk of the faintest blue galaxies located at high redshift (see figs. 18 and 20 in Cowie et al. 1996). Combining these observations with weak lensing, it should be possible to constrain the redshifts of galaxies that are several magnitudes fainter than will be accessible to spectroscopy even with 8–10 m telescopes in the forseeable future.

References

Bahcall, N. 1981, ApJ, 247, 787.

Bonnet, H., Mellier, Y., and Fort, B. 1994, ApJ, 427, L83.

Castander, F., Ellis, R., Frenk, C., Dressler, A., and Gunn, J. 1994, ApJL, 424, L79.

Couch, W., Ellis, R., Malin, D., and MacLaren, I. 1991, MNRAS, 249, 606.

Cowie, L., Hu, E., and Songaila, A. 1995, Nature, 377, 603.

Cowie, L., Songaila, A., Hu, E., & Cohen, J. 1995, AJ, submitted.

Evrard, A. 1989, ApJL, 341, L71.

Fahlman, G., Kaiser, N., Squires, G., and Woods, D. 1994, ApJ, 437, 56.

Fischer, P., Tyson, J.A., Bernstein, G., and Guhathakurta, P 1994, ApJ, 431, L71.

Gioia, I., and Luppino, G. A. 1994, ApJS, 94, 583.

Gioia, I. M., Maccacaro, T., Schild, R.E., Wolter, A., Stocke, J.T., Morris, S. L., Henry, J. P. 1990, ApJS, 72, 567.

Glazebrook, K., Ellis, R., Colless, M., Broadhurst, T., Allington-Smith, J., and Tanvir, N., 1995. MNRAS 273, 157.

Guhathakurta, P., Tyson, J. A., and Majewski, S. 1990, ApJ, 357, L9.

Gunn, J., Hoessel, J., and Oke, J. B. 1986, ApJ, 306, 30.

Gunn, J. 1990, in *Clusters of Galaxies*, eds. W. Oergerle, et al., (Cambridge: Cambridge University Press), p.341.

Henry, J. P., Gioia, I. M., Maccacaro, T., Morris, S. L., Stocke, J. T., and Wolter, A. 1992, ApJ, 386, 408.

Kaiser, N. 1995, ApJ, in press.

Kaiser, N and Squires, G. 1993, ApJ, 404, 441 [KS93].

Kaiser, N., Squires, G., and Broadhurst, T. 1995, ApJ, 449, 460 [KSB].

Kaiser, N., Broadhurst, T., Szalay, A., and Moller, P. 1996, in preparation.

Kneib, J.-P., Mathex, G., Fort, B., Mellier, Y., Soucail, G., and Longaretti, P.-Y. 1994, A&A, 286, 701.

Landolt, A. 1992, AJ, 104, 340.

Luppino, G., and Gioia, I. 1995, ApJL, 445, L77.

Mellier, Y., Dantel-Fort, M., Fort, B., and Bonnet, H. 1994, A&A, 289, L15.

Navarro, J., Frenk, C., & White, S. 1995, MNRAS, 275, 720.

Peebles, J., Daly, R., and Juszkiewicz, R. 1989, ApJ, 347, 563.

Schneider, P. 1995, A&A, 302, 639.

Smail, I., Ellis, R., Fitchett, M., and Edge, A. 1994, MNRAS, 270, 245.

Smail, I., and Dickinson, M. 1995, ApJL, 455, L99.

Smail, I., Ellis, R., and Fitchett, M. 1995, MNRAS, 273, 277.

Squires, G., Kaiser, N., Fahlman, G., Woods, D., Babul, A., Neumann, D., and Bohringer, H. 1995, preprint.

Squires, G. & Kaiser, N. 1995, ApJ, submitted [SK95].

Tyson, J. A., Valdes, F., and Wenk, R. 1990, ApJL, 349, L1.

Tyson, J. A., and Fischer, P. 1995, ApJL, 446, L55.

Vianna, P., and Liddle, A 1995, preprint.

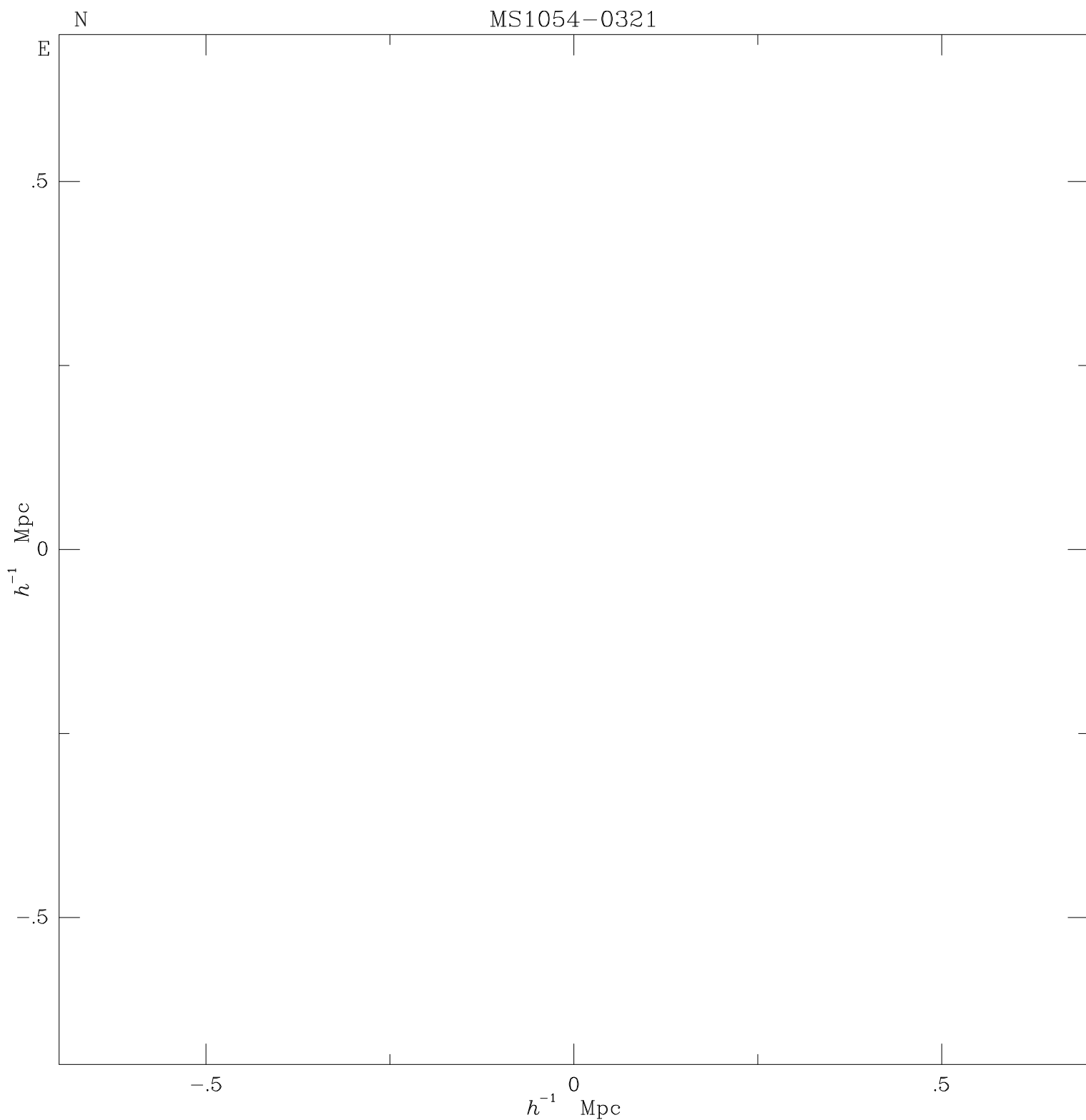White, S., Efstathiou, G., and Frenk, C. 1993, MNRAS, 262, 1023.

N

E

.5

h^{-1} Mpc

0

−.5

−.5

0

.5

h^{-1} Mpc

FIGURE 1 [PLATE 1]. True color image of MS 1054−0321 formed from the B, R, and I CCD frames. This image measures 1536 × 1536 pixels and covers a field of $5'.6 \times 5'.6$ ($1.4h^{-1} \times 1.4h^{-1}$ Mpc at $z = 0.83$).

FIGURE 3 [PLATE 2]. Full 2048×2048 pixel I-band CCD image of MS 1054−03 with the ellipses drawn around all the 2395 objects in the $I > 21.5$ catalog.

FIGURE 5 [PLATE 3]. Contour plot of the surface mass density (black contour lines) and cluster light distribution (white contour lines) overlaid on the 2048^2 pixel optical image of the cluster. Both the mass contours and the light contours have been smoothed with a gaussian of scale length $0''.35$. The image measures $1.86h^{-1}\times1.86h^{-1}\mathrm{Mpc}$, and an $r=0.5h^{-1}\mathrm{Mpc}$ circle centered on the BCG is shown for reference.